

Nontraditional, Safe, High Voltage Rechargeable Cells of Long Cycle Life

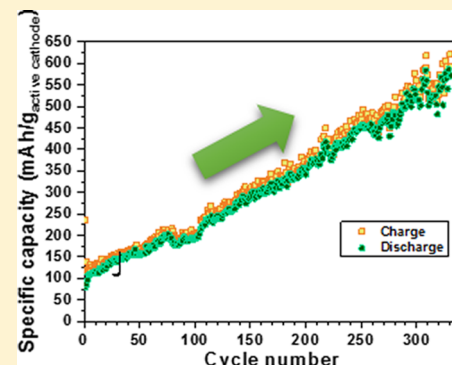
Maria Helena Braga,^{*†‡} Chandrasekar M Subramaniyam,[†] Andrew J. Murchison,[†] and John B. Goodenough^{*†‡}

[†]Materials Science and Engineering Program and Texas Materials Institute, The University of Texas at Austin, Austin, Texas 78712, United States

[‡]LAETA, Engineering Physics Department, FEUP, University of Porto, Porto, Portugal

Supporting Information

ABSTRACT: A room-temperature all-solid-state rechargeable battery cell containing a tandem electrolyte consisting of a Li⁺-glass electrolyte in contact with a lithium anode and a plasticizer in contact with a conventional, low cost oxide host cathode was charged to 5 V versus lithium with a charge/discharge cycle life of over 23,000 cycles at a rate of 153 mA·g⁻¹ of active material. A larger positive electrode cell with 329 cycles had a capacity of 585 mAh·g⁻¹ at a cutoff of 2.5 V and a current of 23 mA·g⁻¹ of the active material; the capacity rose with cycle number over the 329 cycles tested during 13 consecutive months. Another cell had a discharge voltage from 4.5 to 3.7 V over 316 cycles at a rate of 46 mA·g⁻¹ of active material. Both the Li⁺-glass electrolyte and the plasticizer contain electric dipoles that respond to the internal electric fields generated during charge by a redistribution of mobile cations in the glass and by extraction of Li⁺ from the active cathode host particles. The electric dipoles remain oriented during discharge to retain an internal electric field after a discharge. The plasticizer accommodates to the volume changes in the active cathode particles during charge/discharge cycling and retains during charge the Li⁺ extracted from the cathode particles at the plasticizer/cathode-particle interface; return of these Li⁺ to the active cathode particles during discharge only involves a displacement back across the plasticizer/cathode interface and transport within the cathode particle. A slow motion at room temperature of the electric dipoles in the Li⁺-glass electrolyte increases with time the electric field across the EDLC of the anode/Li⁺-glass interface to where Li⁺ from the glass electrolyte is plated on the anode without being replenished from the cathode, which charges the Li⁺-glass electrolyte negative and consequently the glass side of the Li⁺-glass/plasticizer EDLC. Stripping back the Li⁺ to the Li⁺-glass during discharge is enhanced by the negative charge in the Li⁺-glass. Since the Li⁺-glass is not reduced on contact with metallic lithium, no passivating interface layer contributes to a capacity fade; instead, the discharge capacity increases with cycle number as a result of dipole polarization in the Li⁺-glass electrolyte leading to a capacity increase of the Li⁺-glass/plasticizer EDLC. The storage of electric power by both faradaic electrochemical extraction/insertion of Li⁺ in the cathode and electrostatic stored energy in the EDLCs provides a safe and fast charge and discharge with a long cycle life and a greater capacity than can be provided by the cathode host extraction/insertion reaction. The cell can be charged to a high voltage versus a lithium anode because of the added charge of the EDLCs.



1. INTRODUCTION

The Li ion battery of the wireless revolution is limited by its flammable liquid electrolyte.¹ The recent development of a Li⁺-

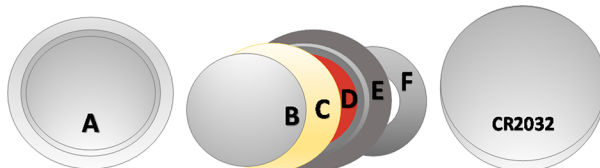


Figure 1. Schematic representation of the all-solid-state cell: (A) stainless steel shell; (B) Li-metal; (C) glass electrolyte in nonwoven paper matrix; (D) SN+LNMO+C+PVDF on Al (double-coated with carbon); (E) spacer; (F) spring.

glass electrolyte with a large energy gap and a Li⁺ working ion conductivity $\sigma_{\text{Li}} > 10^{-2} \text{ S}\cdot\text{cm}^{-1}$ ² and the demonstration^{3,4} that a Li/Li⁺-glass/Li symmetric cell can plate/strip dendrite-free metallic-lithium electrodes at 3 mA·cm⁻² for many thousands of cycles at room temperature with a low plating/stripping impedance has made possible the development of low cost all-solid-state rechargeable battery cells of high energy density and long cycle life.

The energy density of a battery cell is $\langle V(q) \rangle Q(I)$, where $V(q)$ is the discharge voltage at the state of charge q of the cell and the discharge capacity is $Q(I) = \int_0^{Q(I)} dq = \int_0^{\Delta t} I dt$ per weight or volume at a constant discharge current $I = dq/dt$. In a

Received: March 1, 2018

Published: April 24, 2018

conventional rechargeable cell, $Q(I)$ is limited by the solid-solution range of the working ion guest in the oxide host cathode and by the rate of insertion/extraction of the guest into and out of the host; $Q(I)$ decreases with increasing discharge current.

An initial investigation⁴ has demonstrated a low cost cell in which a lithium anode is plated on a carbon-coated copper cathode current collector with MnO_2 relay particles facing the electrolyte and fixing the discharge voltage $V = 3.1$ V. Although this cell is not limited by the conductivity of the guest in a cathode host or its solid-solution range, it is limited by $V(q) \leq 3.5$ V. Moreover, the relative position of the plated lithium with respect to a catalytic relay facing the electrolyte and the relative rates of lithium plating on the cathode and electron arrival from the anode limit the cell's performance; if Li-metal covers a substantial part of the relay surface and if the current is too fast, both the capacity and the cell's voltage decrease.

It has also been shown⁵ that slower-moving electric dipoles in the glass electrolyte induce dendrite-free plating of the working cations from the electrolyte onto an anode current collector or an alkali-metal anode without replenishment from the cathode to give the phenomenon of self-charge as well as a Coulombic efficiency of a single charge/discharge cycle of over 100%. This property of the glass is used to provide the nontraditional, safe, high voltage rechargeable cells of long cycle life reported in this paper.

We demonstrate here a room-temperature, all-solid-state, high voltage cell of long cycle life with a tandem electrolyte consisting of a Li^+ -glass electrolyte of ref 2 in a paper nonwoven matrix contacting a lithium anode and a succinonitrile (SN) plasticizer⁶ coating a low cost high voltage oxide host cathode into which Li^+ is inserted reversibly over a large solid-solution range. A schematic representation of the cell assembly is shown in Figure 1. The oxide cathode contacts the cathode current collector on one side and, on the other side, a plasticizer that is not oxidized below 5 V versus Li^+/Li^0 . The plasticity of the plasticizer retains its contact with the cathode particles through the volume changes that occur during a charge/discharge cycle over thousands of cycles to provide a long cycle life. A fast charge/discharge cycle is achieved because electric dipoles in both the Li^+ -glass and the plasticizer induce short-displacement electrode/electrolyte reactions of the ionic component while the electronic component remains between the two electrodes as in a conventional cell. The cell capacity increases with cycle number until it stabilizes (not shown) at a value higher than the theoretical capacity of the cathode host oxide.

2. EXPERIMENTAL SECTION

2.1. Synthesis of Cathode Host F-Doped Li-Rich Spinel. Nominal $\text{Li}_x\text{Ni}_{0.5-y}\text{Mn}_{1.5-z}\text{O}_{4-x-\delta}\text{F}_x$ with $x = y + z \approx 0.36$ and $\delta \approx 0.36$ (LNMO) was prepared. All chemical precursors utilized were 99.99% pure and purchased from Sigma-Aldrich. The $\text{Ni}_{0.5}\text{Mn}_{1.5}\text{O}_{3-\delta}(\text{OH})_{1+\delta}$ (NMO) precursor was prepared by a solvothermal method. The transition metal acetates, $\text{Ni}(\text{CH}_3\text{COO})_2 \cdot 4\text{H}_2\text{O}$, $\text{Mn}(\text{CH}_3\text{COO})_2 \cdot 4\text{H}_2\text{O}$, and urea (chelating agent), were dissolved in 50 mL of ethanol (solvent). The obtained homogeneous solution was then transferred to a 90 mL Teflon-lined stainless steel autoclave and heated in a muffle furnace at 200 °C for 24 h. After cooling to room temperature, the obtained slurry was centrifuged/washed several times with ethanol and vacuum-dried at 60 °C overnight. A stoichiometric amount of ground lithium carbonate (Li_2CO_3) to lithium fluoride (LiF , 10% excess) was mixed with the product and heated to 800 °C for 15 h in air. High resolution neutron powder diffraction (NPD) patterns of the product were indexed and

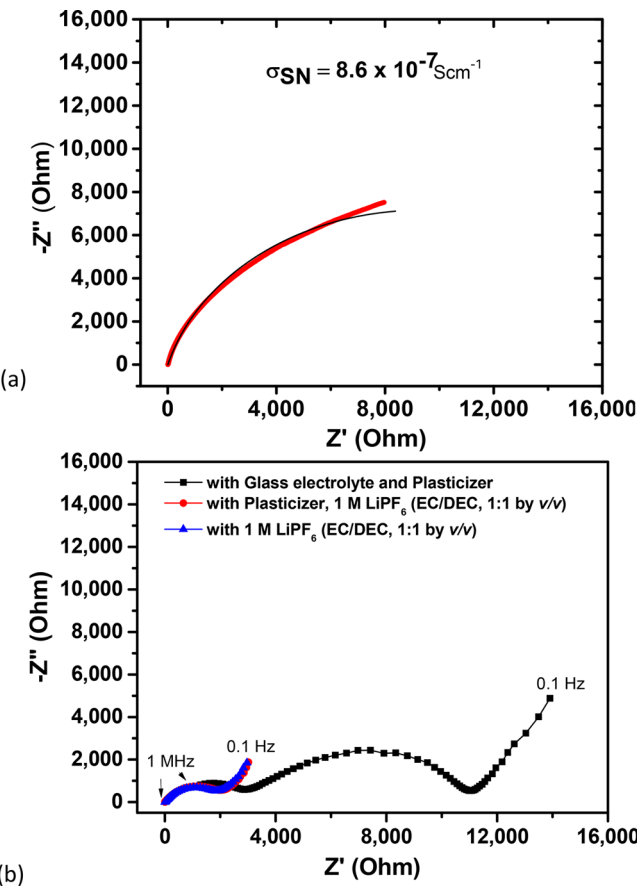


Figure 2. Impedance spectra (PEIS) of succinonitrile (SN) and fresh cells: (a) succinonitrile (SN) experimental thick red line and calculated with equivalent circuit (black thin line); (b) fresh cells before cycling: (squares) Li/Li-glass in paper/SN+LNMO+C+PVDF—this cell was rested for 1 month to optimize the interfaces; (circles) Li/liquid electrolyte+Celgard/SN+LNMO+C+PVDF; (triangles) Li/liquid electrolyte+Celgard/LNMO+C+PVDF.

refined to determine a spinel phase ($Fd\bar{3}m$) and a layered phase ($C2/m$) with a measured ratio of 78 wt % spinel phase and 22 wt % layered phase containing Li_2MnO_3 planes. The NPD data were collected on ECHIDNA, the high resolution neutron powder diffractometer at the Open Pool Australian Light-water (OPAL) research reactor of the Australian Nuclear Science and Technology Organisation (ANSTO)⁷ with a neutron beam wavelength of 1.62161(5) Å, determined by using the $\text{La}_{1.6}\text{NIST}$ standard reference material 660b (in the Supporting Information, Figure S1 and Table S1).

2.2. Synthesis of a Ba-Doped Li^+ -Glass Electrolyte. Nominal dielectric amorphous-oxide (glass) Li^+ electrolytes $\text{Li}_{2.99}\text{Ba}_{0.005}\text{Cl}_{1-2x}\text{O}_{1+x}$ with $0 \leq x < 1$ were obtained in a wet synthesis, as described previously^{2,3} from commercial precursors LiCl (>99%, Merck), Li(OH) (98%, Alfa Aesar), and $\text{Ba(OH)}_2 \cdot 8\text{H}_2\text{O}$ (98.5%, Merck). The glass products were dried by HCl and/or Cl_2 evaporation at lower temperatures and the loss of the OH^- as H_2O from the hydroxide crystalline precursor phases below 230 °C as previously shown;² the reaction leaves an amorphous solid glass containing Li_2O and LiO^- electric dipoles. The samples obtained after synthesis were ground with an agate mortar and pestle while mixed in absolute ethanol. Nonwoven paper separators of about 40–60 μm thick were immersed in the electrolyte–ethanol mixture and dried at about 180 °C in an argon-filled glovebox (MBraun, Germany).

2.3. Preparation of the Cathode. The cathode was prepared by mixing the LNMO particles with carbon Super P as a conducting agent and polyvinylidene fluoride (Sigma-Aldrich) (PVDF) as a binder in a weight ratio of 8:1:1 with *N*-methyl-2-pyrrolidone (NMP) as solvent.

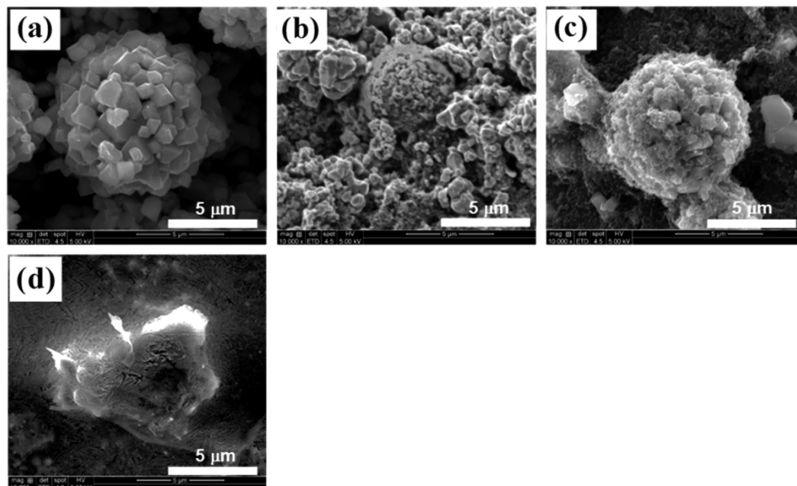


Figure 3. FESEM of (a) pristine F-doped LNMO cathode; (b) cathode with Super P Carbon (8:1:1) and with PVDF; (c) cathode with Super P Carbon (8:1:1) and PVDF and covered with SN (7:3); (d) cathode with glass electrolyte and SN after cycling and detachment of paper matrix containing glass electrolyte. Magnification 10,000 \times .

The slurry was mixed in a plenary mixer (Kurabo Mazerustar, Japan) and coated on one side of double-sided carbon-coated aluminum foil. Finally, the cathode was dried at 120 °C overnight in a vacuum oven.

A mixture of succinonitrile (SN) plasticizer and LiClO₄ salt in a molar ratio of 20:1 was heated in an argon-filled glovebox (MBraun, Germany) to get a transparent solution. The LiClO₄ was mixed into the SN, but the conductivity of the SN did not increase as much as expected⁸ owing to not melting the LiClO₄ prior to mixing it with SN. The cathode was prepared by dropping the solution of succinonitrile-based material that was heated to $T \geq 57$ °C onto a prepared cathode surface that faced the glass electrolyte in a paper matrix. The prepared cathode consisted of oxide host particles and carbon contacting the cathode current collector. The SN coated the entire surface of the active cathode particles without intruding into their contact with the cathode current collector. After cooling down to room temperature, the succinonitrile-coated cathode was flexible. The weight ratio of the cathode to the SN was 7:3. The loading of the active cathode material on the aluminum foil of the all-solid-state cells was 0.1–0.25 mg, which corresponds to about 0.20–0.35 mg·cm⁻² (diameters 0.79 and 0.95 cm) of active material.

2.4. Cell Assembly and Testing. The electrochemical performances of Li/LNMO CR2032 coin cells with three different electrolytes were compared; each cell was assembled in an argon-filled glovebox (MBraun, Germany).

2.4.a. Li/Li-Glass in Paper/SN+LNMO+C+PVDF All-Solid-State Cells. Half-cells were assembled with the afore-prepared cathode as the working electrode and Li-metal foil as the counter/reference electrode. Circular lithium-metal anodes with a 1.2 cm diameter and 0.2–0.3 mm thick were deposited on stainless steel and then covered with a paper matrix containing the glass electrolyte. Finally, the cathode coated with SN was added as well as a spacer and spring, as shown in Figure 1. We used half a drop of 1 M LiClO₄ in propylene carbonate (PC) and diethyl carbonate (DEC) 1:1 to facilitate the contact between the paper and the cathode SN surface; no excess liquid was ever found in the cell; and when cells were opened after cycling, the paper was strongly attached to the SN surface of the cathode coat, making it very hard to detach.

2.4.b. Li/Liquid Electrolyte with Celgard/SN+LNMO+C+PVDF. For comparison, we assembled a cell in which the glass electrolyte in a paper matrix was replaced by a Celgard polypropylene film as a separator impregnated with a few drops of commercially available 1 M LiPF₆ in 1:1:1 (V/V/V) of ethylene carbonate (EC)/diethyl carbonate (DEC)/dimethyl carbonate (DMC) as electrolyte.

2.4.c. Li/Liquid Electrolyte and Celgard/LNMO+C+PVDF. For additional comparison, we assembled a cell without the plasticizer (succinonitrile-SN) on the cathode's surface; the glass electrolyte in

the paper matrix was replaced by a Celgard polypropylene separator film impregnated with a few drops of commercially available 1 M LiPF₆ in 1:1:1 (V/V/V) of EC/DEC/DMC as electrolyte.

All three assembled cells were electrochemically tested in a battery testing analyzer (LAND, China CT2001A) at constant specific current densities and voltages between 2.0/2.5/3.0 and 4.5/4.8 V or 2.3/3.0 and 5.0 V. Moreover, the cell discharge currents were tested with red and white LEDs having a lighting current ranging from 0.1 mA $\leq I_{\text{dis}} \leq$ 1 mA and input lighting voltages $V \geq 1.5$ V and $V \geq 3$ V, respectively, as well as with the blue LED having a lighting current ranging from 0.005 mA $\leq I_{\text{dis}} \leq$ 1 mA and input lighting voltages $V \geq 2.4$ V and Fluke multimeters. A Solartron electrochemical workstation was used to perform potentiostatic electrochemical impedance spectroscopy (PEIS) in the frequency range from 1 MHz to 10 mHz against Li⁺/Li⁰ at open circuit voltage with an AC amplitude of 10 mV, Figure 2. An equivalent circuit containing a resistor with resistance R_1 in series with a capacitor with capacitance C in parallel with a second resistor of resistance R_2 was used to calculate the black line in Figure 2a. The ionic conductivity of the SN, σ_{SN} , was calculated as $R_2 = (1/\sigma_{\text{SN}}) \cdot d/A$, in which d is the thickness of the SN and A the surface area. Gold blocking electrodes were used.

2.5. Material Characterization. The nominal fluorine-doped Li-excess spinel cathodes were analyzed for phase identification as well as surface and electrochemical characterization. Field-emission gun-scanning electron microscopy (FEI Quanta 650) coupled with energy dispersive X-ray spectroscopy (EDS, Bruker) operated at 5 kV and 10 μ A was used to visualize and study the structural morphologies and atomic distribution. All surfaces were gold plated prior to SEM observation to prevent charge accumulation since most of the materials are not good electronic conductors.

3. RESULTS AND DISCUSSION

The nominal composition of the active oxide host cathode particles was Li_{1.36}Ni_{0.49}Mn_{1.15}O_{3.28}F_{0.36} (LNMO) that disproportionated into 78 wt % spinel phase LiNi_{1/2}Mn_{3/2}O_{3.8}F_{0.2} and 22 wt % Li-rich, F-doped layered phase containing Li₂MnO₃ planes separated by Li⁺ and Ni²⁺ ions. Segregation of a Ni²⁺-rich second phase occurs reversibly above 700 °C in the spinel Li[Ni_{0.5}Mn_{1.5}]O₄.^{9–11} Li⁺ conduction is fast in both spinel and layered-oxide phases.

Figure 2a shows a high impedance of the plasticizer (SN), which makes it a barrier to fast Li⁺ conduction. Figure 2b reinforces the hypothesis of SN as a barrier. In the cell that contained a liquid electrolyte and plasticizer, no more than the

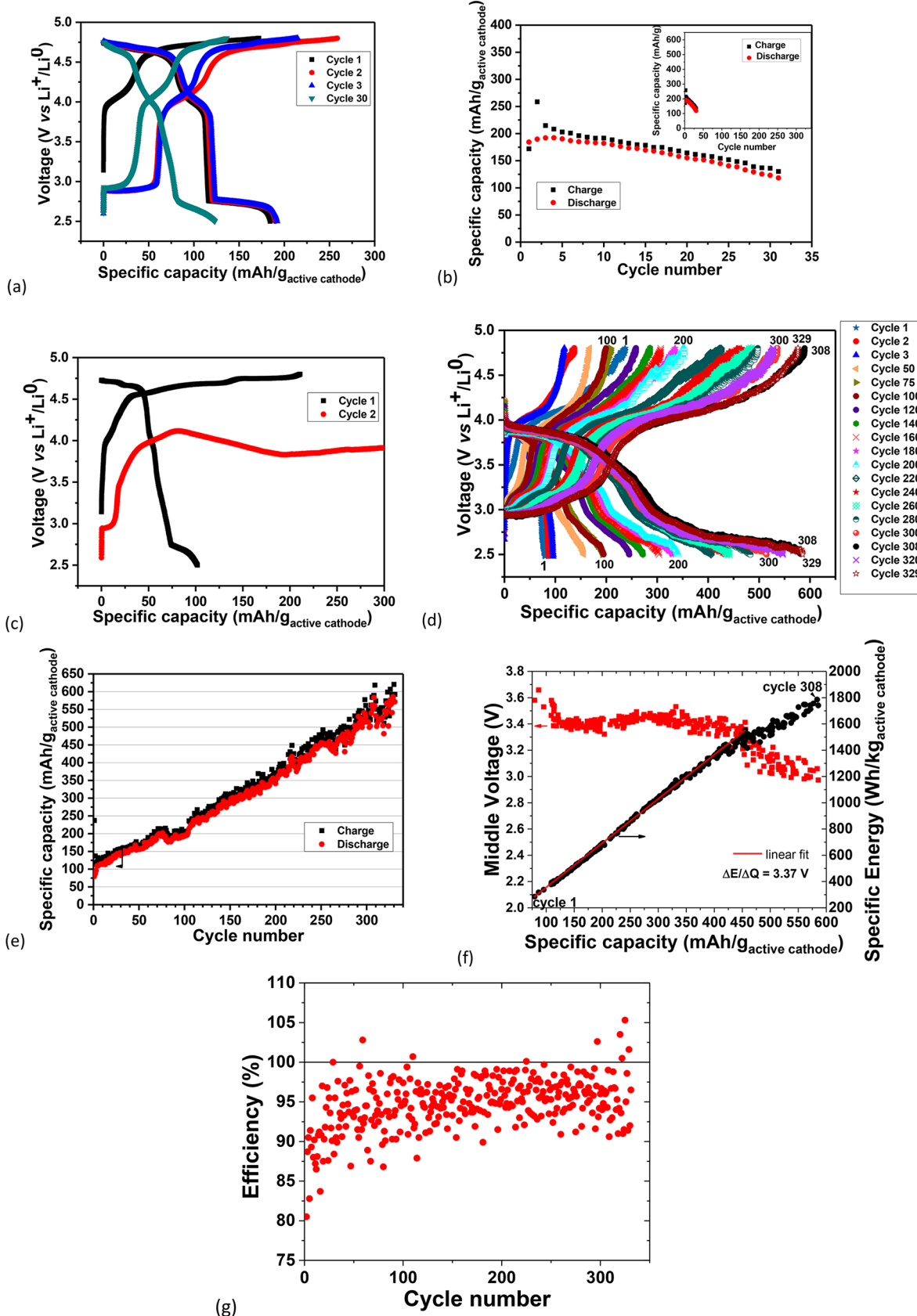


Figure 4. Comparison between the electrochemical performances of three half-cells prepared with cathodes from the same batch and differing in the type of electrolyte and separator. Cycling performance of (a, b) Li/liquid electrolyte+Celgard/LNMO+C+PVDF; (c) Li/liquid electrolyte+Celgard/SN+LNMO+C+PVDF; (d–g) Li/Li-glass in paper/SN+LNMO+C+PVDF. Specific current: 23 mA·g⁻¹. Specific capacity, current, and energy are per mass of active cathode material (layered-spinel composite).

Table 1. Electrochemical Characteristics of Different Classes

cathode	framework	initial plateau voltage (V)	capacity in liquid electrolyte (mAh g ⁻¹)	
LiNi _{1/2} Mn _{3/2} O ₄	spinel	4.7	147 (120) ^a	
LiMn ₂ O ₄	spinel	4.1	147 (120) ^a	
LiCoO ₂	layered	4.2	272 (140) ^a	
LiNi _{1/3} Mn _{1/3} Co _{1/3} O ₂	layered	4.0	272 (200) ^a	
LiFePO ₄	olivine	3.45	170 (160) ^a	
LiFe _{1/2} Mn _{1/2} PO ₄	olivine	3.4/4.1	170 (160) ^a	
cathode	framework	initial plateau voltage (V)	capacity in glass electrolyte (mAh g ⁻¹)	
LNMO (Li _{1.36} Ni _{0.49} Mn _{1.15} O _{3.28} F _{0.36})		78 wt % spinel 22 wt % layered	302 (cycle 308; cutoff: 3 V) 170 (cycle 316; cutoff: 3 V)	
cathode	theoretical capacity (mAh g ⁻¹)	experimental capacity (mAh g ⁻¹)	experimental average voltage (V)	experimental specific energy (Wh kg ⁻¹)
LiNi _{1/2} Mn _{3/2} O ₄ ¹³ (liquid electrolyte)	147	135 (cutoff: 3.5 V), first cycle	4.7 (cutoff: 3.5 V), first cycle	635 (cutoff: 3.5 V), first cycle
LiNi _{1/2} Mn _{3/2} O _{3.8} F _{0.2} (glass electrolyte)	114 ^b	224 (cutoff: 3.5 V), cycle 308	3.8 (cutoff: 3.5 V), cycle 308	908 (cutoff: 3.5 V), cycle 308

113 (Figure 4a)

^aTheoretical (experimental) values; in parentheses, the practical specific capacity of the electrode for the *first cycle*. ^bThe spinel contributes 78 wt % for the nominal composition (see the Supporting Information). The theoretical composition is $0.7 \times 146 = 114$ mAh g⁻¹.

liquid-electrolyte semicircle is observed in the Nyquist spectrum from 1 MHz to 0.1 Hz. The plasticizer covering the cathode's surface creates a quasi-blocking electrode characterized by a Warburg impedance element associated with a charge-transfer resistance and a double-layer capacitance.

The PEIS spectrum corresponding to the Li/Li-glass in paper/SN+LNMO+C+PVDF shows that the conductivity of the bulk glass in the paper is very similar to that of the liquid electrolyte in the presence of the Celgard separator. However, an additional semicircle is observed, corresponding to the conductivity of the Li⁺ ions across the Li⁺-glass/SN and Li⁺-glass/Li interfaces where EDLCs had been formed during 1 month of cell resting. It is evident that at the glass/anode and glass/plasticizer interfaces where either excess Li⁺ ions or negatively charged Li⁺ deficiencies are concentrated forming EDLCs, the Li⁺ ion movements are slowed down by strong Coulombic forces. This impedance is by itself very large, ≈ 11 k Ω , and addition of the high impedance of the SN makes it impossible for ionic currents to deliver the high currents needed to light a red or a white (higher current) LED. In a traditional cell with a liquid electrolyte, the EDLCs formed at the electrode/electrolyte interfaces to equilibrate the chemical-potential difference between anode/cathode and electrolyte are discharged as soon as the external electric circuit is closed and the internal electric fields in the EDLCs decrease. In an electrochemical cell containing electric dipoles in the electrolyte, there is an extra electric field that remains different from zero even after charge/discharge due to retention of the alignment of the dipoles.

Figure 3 shows SEM images of (a) the cathode with just the active material, (b) the cathode with the addition of carbon and PVDF, (c) the cathode with the plasticizer SN coating the cathode of (b), and (d) the cathode with the glass electrolyte (bright area) on the SN after cycling. Carbon makes electrical contact with the active material and with the aluminum current collector. The plasticizer coats the cathode's entire outer surface, including the active material, as observed by comparison between (a), (b), and (c) as well as Figures S2 and S3 of the Supporting Information, but it does not intrude into the contact between the cathode current collector and the

active cathode particles (see Figures S3 and S4 for more information).

Figure 4 shows the charge/discharge performances of three cells with different electrolytes. The electrochemical cell with an organic-liquid electrolyte, (a) and (b), showed an initial discharge voltage of about 4.7 V, but the capacity faded rapidly during the first 30 cycles because the liquid electrolyte is oxidized and forms an ionic-insulator solid–electrolyte interphase (SEI) layer. The steps at approximately 4.1, 2.7, and 2.1 of Figure 4a, b, and c are, respectively, from the Mn⁴⁺/Mn³⁺ couple of the spinel phase and layered phases; the step at $V \approx 4.7$ V, which is clear in Figure 4c, shows a small change on passing from the Ni³⁺/Ni²⁺ to the Ni⁴⁺/Ni³⁺ couple during charge, as has been well-documented for the Li[Ni_{1/2}Mn_{3/2}]O₄ spinel phase.^{9–11} The cell in Figure 4d–g shows a set of equilibria in which the layered phase is predominant, as reported in ref 12. Table 1 compares the electrochemical behavior of the Li-rich F-doped LNMO with the glass-plasticizer tandem electrolyte to that of other cells with oxide host cathodes.

The electrochemical cell with the organic-liquid electrolyte contacting the anode and a plasticizer contacting the cathode (c) showed a rapid reduction of the charging voltage and no discharge current by the second cycle, indicating metallic lithium was not plated on the anode from the mobile cations in the liquid electrolyte. On the other hand, the electrochemical cell with the glass electrolyte and plasticizer (SN) (Figure 4d–g) exhibited with increasing number of cycles an increase of both the cell's capacity at 2.5 V, from 79 to 586 mAh·g⁻¹. Figure 4f shows as a function of the specific capacity of the active cathode, and therefore of cycle number, not only an almost constant middle voltage of about 3.37 V, but also an important increase in the gravimetric energy density per mass of active material. The energy efficiency was 86% for cycle 329, while for the first cycle it was 30%. The Coulombic efficiency, defined as $Q_{\text{dis}}/Q_{\text{ch}}$, has an average tendency to increase with cycle number, as shown in Figure 4g. For more information on the cycling performance of four additional cells, see Figures S5–S8.

Figure 5 shows the cycling performance of a Li/Li-glass in paper/SN+LNMO+C+PVDF cell at 153 mA·g⁻¹ active ma-

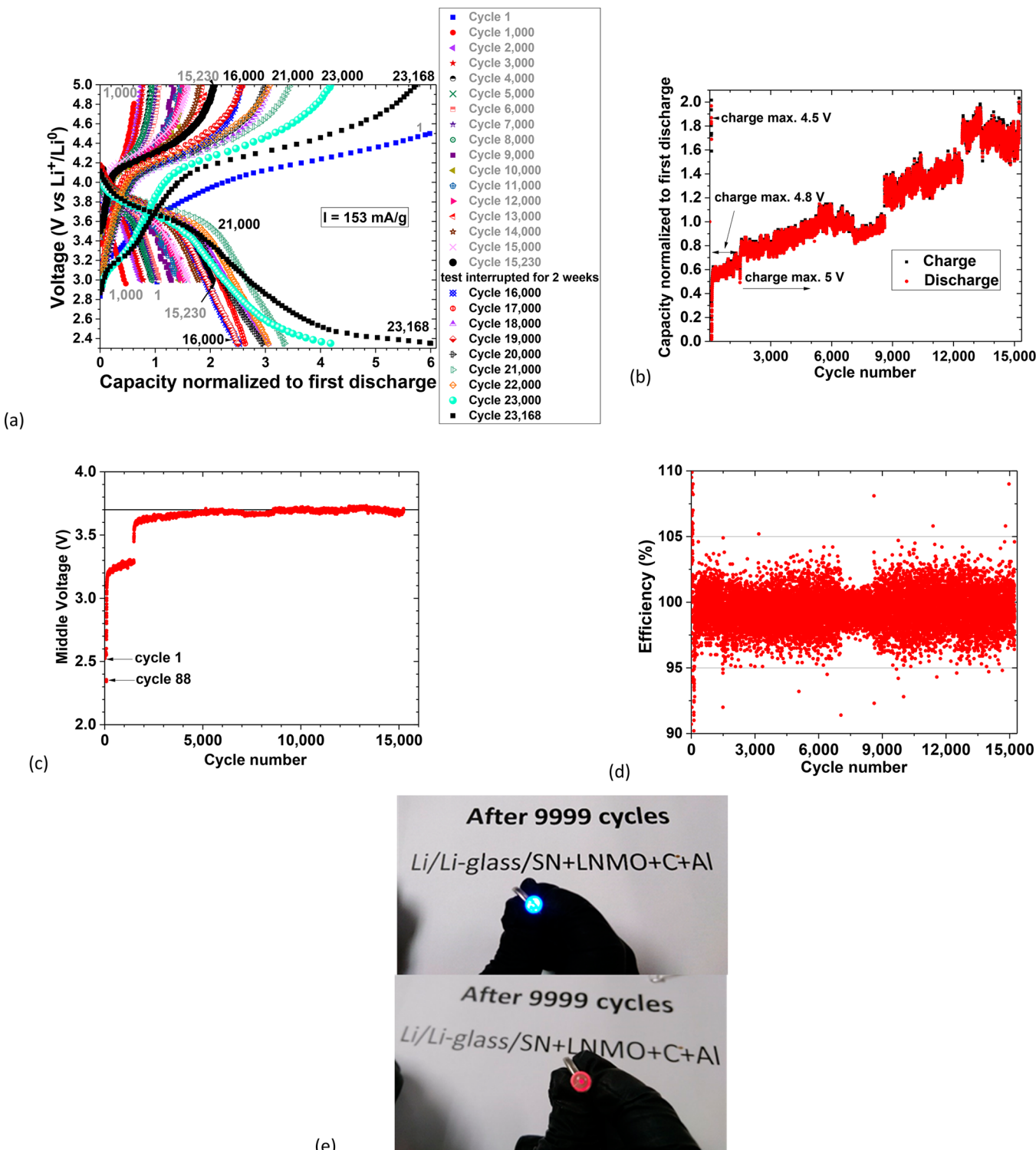


Figure 5. Electrochemical performance of a Li/Li-glass in paper/SN+LNMO+C+PVDF: (a–d) Cycling performances; specific current: 153 mA g^{-1} active material. (e) Lighting of blue and red LEDs after the 9999th discharge. The discharge capacities are smaller than those of the first cycle up to the 5000th cycle and then increased to cycle 15,230 when the experiment was interrupted for 2 weeks. When the experiment reinitiated, the discharge capacity shown was very similar to the capacity achieved before the interruption. From 17,000 to 23,168 cycles, the discharge capacities do not cease to increase.

terial cycled 23,168 times with two interruptions: (1) after the 9999th discharge to show the cell lit a blue and a red LED, shown in (e); (2) 2 weeks during which the cell was at open circuit voltage; after this last period, the discharge cutoff decreased to 2.35 V and the cell was tested in another channel

for quality control. In (a), the discharge capacity normalized to that of the first discharge increases with cycle number after the first 90 cycles, as shown in (b). In the first 90 cycles, the maximum charge voltage was 4.5 V, leading to middle voltages of 2.34–2.58 V and (c) discharge capacities that vary between

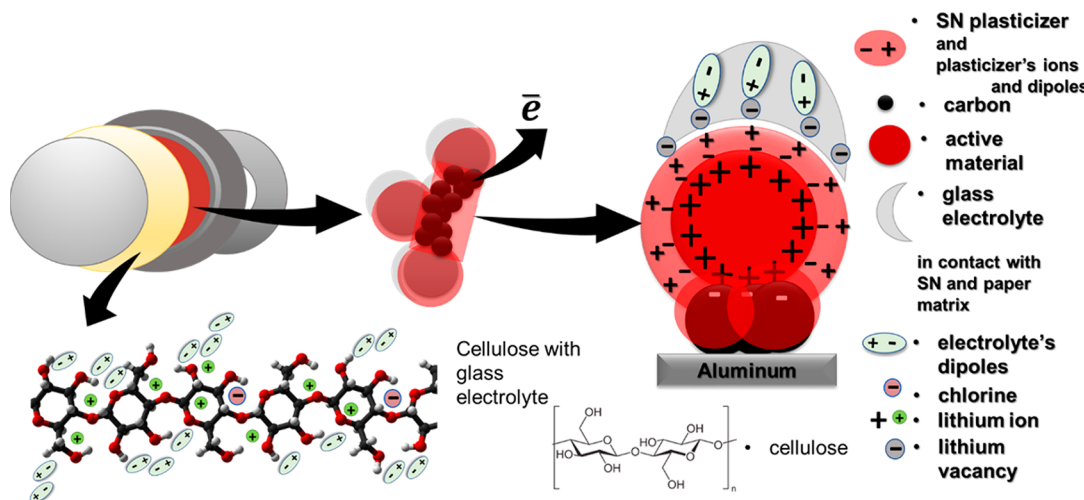


Figure 6. Schematic representation of the charge process. The active particle on the right side represents the hypothetical charge on the particle of Figure 3d. All of the EDLCs at the cathode side are represented in the schematics. While charging, electrons and Li⁺ leave the active particles. While ions accumulate at the surface with the plasticizer, the electrons are transported through the carbon and current collector to the external circuit.

approximately 2 and 200% of the first discharge capacity, showing that the capacity obtained was not due to charge/discharge of the spinel phase (see Figure S6 cycle 100 for a similar cycle with another cell). At approximately 2000 cycles, the capacity is 0.8 of the first discharge capacity and the middle voltage is 3.6 V (a–c). At 15,233 cycles, the capacity increased to twice the first discharged capacity and the middle voltage is stable at 3.7 V. The Coulombic efficiency is normally less than 100% for an incomplete discharge. The Coulombic efficiency shown in (d) corresponds to discharge to 3 V, yet many cycles are in excess of 100%.

Figure 6 shows a schematic drawing of the charging process. At the anode, not shown in the drawing, the mobile Li⁺ ions accumulate rapidly in the glass electrolyte side of the glass/anode interface during charge; the slower-moving electric dipoles in the ferroelectric glass¹⁴ also move across the electrolyte to the anode/electrolyte interface to enhance the electric field inside the electrolyte; the readjustment of the equilibrium of the electrochemical potentials across the anode heterojunction with the electrolyte then induces a plating of additional surface Li⁺ onto the lithium anode (see Figures S9 and S10 and text on self-charge). Without replenishment of the glass electrolyte Li⁺ from the cathode, the electrolyte becomes negatively charged, and the Li⁺ deficiency at the glass/plasticizer interface is not reduced, but charges the Li⁺-glass electrolyte/plasticizer EDLC. During charge, this process adds to the plating of electrolyte Li⁺ as Li⁰ onto the lithium anode and induces additional electrons transported from the cathode to the anode. Moreover, it charges the EDLC of the Li⁺-glass electrolyte/plasticizer interface (Figure 7a). In the plasticizer, the positive charges of the LiClO₄ salt and/or of the plasticizer electric dipoles are moved or rotated toward the surface that faces the glass electrolyte and the negative charges are rotated toward the surface facing the active material where Li⁺ ions from the cathode particles accumulate at its surface as the active material is oxidized during charge.

Figure 7a shows the result of a discharge in which electrons transported from the anode to the cathode in the external circuit induce a stripping of Li⁺ from the lithium anode back to the Li⁺-glass electrolyte, which reduces the net negative charge

of the electrolyte. At the cathode, the added electrons induce reinsertion of the Li⁺ accumulated at the plasticizer/cathode interface back into the cathode host. The plating/stripping and extraction/insertion reactions at the two electrodes are fast, as they involve only a small displacement of the Li⁺ ions. This process, which reduces the internal EDLCs at the electrode/electrolyte interfaces, may be aided by a cooperative partial rotation of the plasticizer electric dipoles. The rate of charge/discharge is limited by the Li⁺ conductivity inside the active cathode material. It has been shown⁵ that plating of electrolyte Li⁺ onto the anode is faster than stripping and that not all of the plated Li during charge is stripped back during the subsequent discharge. Why the capacity of our cells increases with cycle number over an initial aging time appears to reflect primarily an increase with time in the dipole polarization contribution to the anode and Li⁺-glass electrolyte/plasticizer EDLCs. Figure 7b shows a lit LED corresponding to an initial cell internal resistance smaller than 2 kΩ (for $I_{dis} = 0.1$ mA at 3 V) before charging, which is the same order of magnitude as the resistance of the Li⁺ hopping in the bulk glass electrolyte in the paper matrix shown in Figure 2b (diameter of the semicircle at high frequencies on the real impedance axis). Figure 7c shows the charge/discharge cycles of a high voltage cell discharged at 46 mA g⁻¹ of the active material. The first cycle shows a reduced Coulombic efficiency that is not due to the formation of an SEI layer as in a traditional cell. If an SEI layer was formed, the Coulomb efficiency would drop drastically with increasing number of cycles, as is shown in Figure 4a and b for a cell with a liquid electrolyte. The origin of the reduced Coulombic efficiency in the first cycle of the all-solid-state cell (which may reflect structural changes in the active material) has not been totally determined, although it might be due to initial lack of polarization of the electrolyte and plasticizer and interface disorder. The subsequent steady increase in capacity with cycle number is typical of the self-charge capability due to spontaneous polarization of the Li⁺-glass ferroelectric electrolyte.⁵ In cycle 316, the cell's capacity was more than double the initial capacity and the plateau voltage was also increased. The cell was still running after more than 1600 cycles. Figures S5–S8 show cycling performances of four additional cells, including

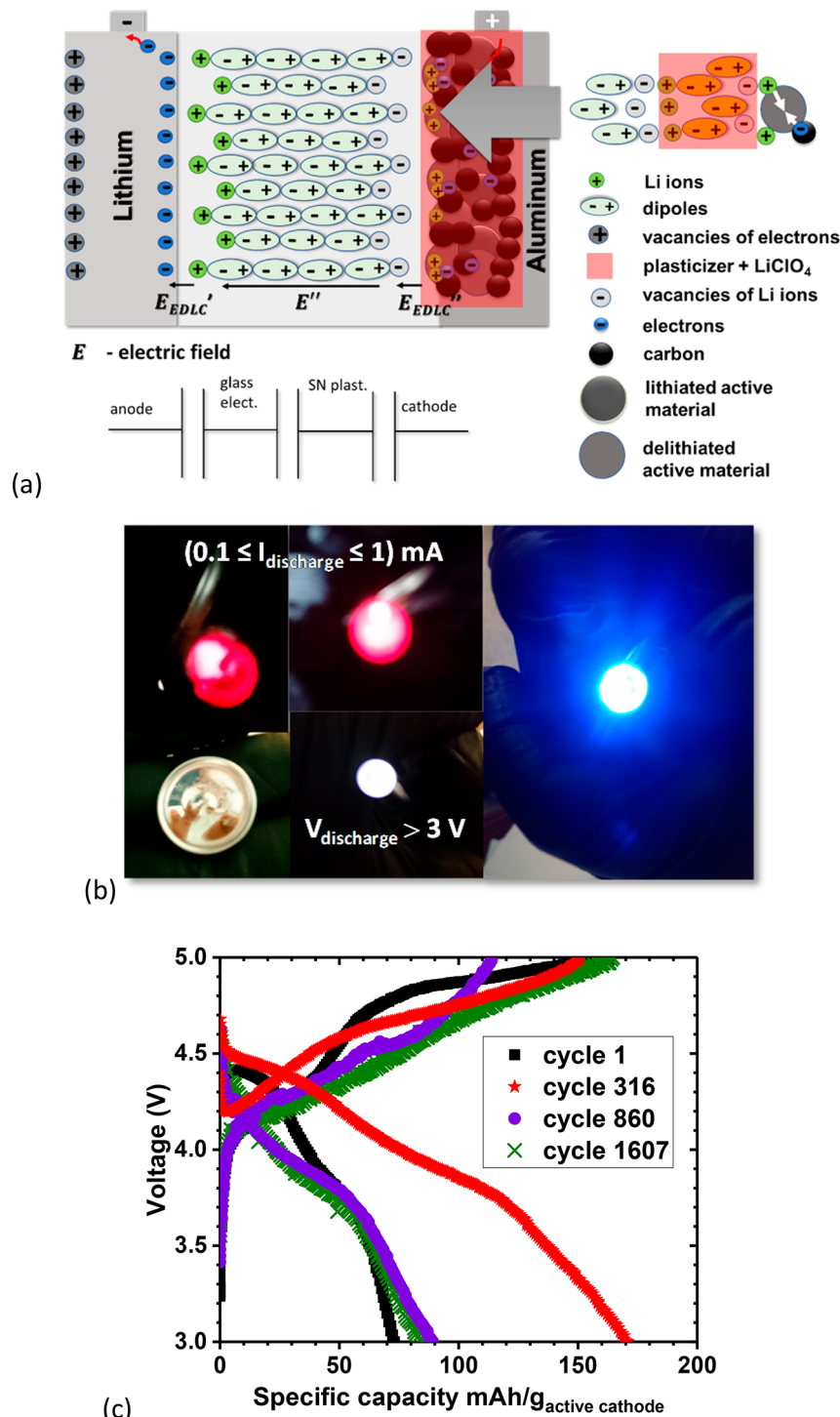


Figure 7. Discharge process. (a) Schematic representation showing the discharge process in which the electrons from the external circuit and Li ions travel back from the surface with the plasticizer to the active particle, quickly discharging the EDLC at the interface plasticizer/cathode and slowly discharging the EDLC Li-glass/plasticizer that is not accessed by electrons and discharges by ion/vacancy diffusion and dipole rotations; (b) LEDs lit with the cell in part c before charge. (c) Cycling from 3.0 to 5.0 V at 46 mA/g of active material. Cycle 316 shows a small plateau corresponding to the spinel phase. Specific capacity, current, and energy are per mass of active cathode material (layered-spinel composite).

one that has been cycling over 5000 times with increasing capacity at 77 mA·g⁻¹ of the active material.

The increase of capacity, and therefore of the energy density, with increasing cycle number eventually gives a capacity that is greater than the theoretical capacity of the oxide host cathode particles. This extraordinary observation indicates that there must be a storage of charge in addition to that in the active

particles. The additional stored charge can only be electrostatic storage in an EDLC as in a supercapacitor. The cell in Figure 4d–g shows a capacity at 308 cycles of 586 mAh·g⁻¹ (cutoff voltage of 2.5 V). For this cathode, the theoretical capacity is 241 mAh·g⁻¹ (cutoff voltage of 2.5 V), which is very close to the capacity of the first charge 237 mAh·g⁻¹ (as expected for these high voltage cathodes), then $Q = 586 - 237 \text{ mAh} \cdot \text{g}^{-1} =$

$349 \text{ mAh}\cdot\text{g}^{-1} = 1,256 \text{ C}\cdot\text{g}^{-1}$ and, therefore, $Q = C_{\text{equivalent}}V = 1,256 = C(4.8-2.5) \Rightarrow C_{\text{equivalent}} = 546 \text{ F}\cdot\text{g}^{-1}$ of the active cathode material or $C_{\text{equivalent}} = 137 \text{ mF}$ (not accounting for the energy lost in the internal resistance), where Q is the capacity, $C_{\text{equivalent}}$ is the capacitance of the equivalent capacitor, and V is the voltage of the cell.

We propose that the capacity increases due to the increasing alignment of the dipoles in the electrolyte, increasing not only the capacity of the EDLCs and, as a consequence, the self-charge, but also reducing the resistance of the ion hopping within the electrolyte. Our model to account for our electrochemical data is based on two concepts: (1) The interface between two solids in contact with one another is a heterojunction across which an electric-double-layer capacitor (EDLC) forms to make equal the electrochemical potentials (Fermi levels) of the two materials. (2) The electric field inside an electrochemical cell having a solid electrolyte containing both fast mobile cations and slower-moving electric dipoles (as in the dielectric glass electrolyte contacting the anode in our experiments) may change over time from that developed initially by the mobile cations because of a changing dielectric constant imposed by the spontaneous alignment of electric dipoles characteristic of ferroelectric materials. To this alignment of the dipoles corresponds a certain surface charge equal to $Q_f = \epsilon_r Q_i$, where Q_i is the capacity of the EDLC before alignment and Q_f is that after alignment and $\epsilon_r \approx 10^7$ is the dielectric constant at room temperature. The consequences of this interplay and the restriction of the Fermi levels across an electrode/electrolyte interface are subtle; since all of the voltages ΔV at the electrode/electrolyte interfaces must be kept constant because all voltages across the EDLCs are restricted to the necessary value to align the Fermi levels of the electrolyte/electrode heterojunctions and since $Q = C\Delta V$, then, if Q increases at the electrolyte's surfaces, C has to increase proportionally. However, $C = \epsilon_0 A/d$, where ϵ_0 is the vacuum's permittivity and A is the surface area, can only vary by decreasing the thickness d , which was already of the order of 3.8 Å. Therefore, the electrons attracted to the anode surface by the added electrolyte charging have a greater probability to tunnel to the electrolyte Li^+ at the interface to plate the cations, thereby reducing the increase in Q_i . The plating on the anode by this process represents a self-charge that can add to a charge supplied by an applied charging power, thereby increasing the Coulombic efficiency to $Q_{\text{dis}}/Q_{\text{ch}} > 100\%$. This process can happen during both charge and discharge. Moreover, the extra negative charge, accumulated as Li^+ vacancies at the electrolyte/plasticizer interface, will contribute to charge the corresponding EDLC, which contributes to the extra electrostatic discharged capacity. There is conservation of the total charge in the battery cell.

CONCLUSIONS

An all-solid-state rechargeable battery cell with a lithium anode and a conventional oxide host as the active material of the cathode can provide a low cost, high voltage, room-temperature cell of high gravimetric energy density, fast charge and discharge, and long cycle life. The solid electrolyte of the cell consists of a Li^+ -glass electrolyte contacting the anode and a plasticizer coating the cathode. Electric dipoles in the Li^+ -glass and the plasticizer are oriented by the internal electric fields generated during charge by a redistribution of the working ions in the Li^+ -glass electrolyte and by the extraction of Li^+ from the cathode host particles. The plasticizer retains the extracted Li^+

at the surface of the active cathode host particles, and orientation of its dipoles creates an EDLC at the plasticizer/cathode and the plasticizer/ Li^+ -glass interfaces. A contribution to the anode/ Li^+ -glass EDLC created during charge can induce plating of the Li^+ -glass mobile cation onto the lithium anode to provide a faradaic component to the electrostatic charge stored in an EDLC at the anode/ Li^+ -glass interface. The discharge of EDLCs adds to the faradaic capacity of the high voltage oxide host cathode particles to yield a large specific energy storage. Retention at the active particle surface of the Li^+ extracted from the cathode active particle host during charge and prevention of Li^+ transport across the Li^+ -glass/plasticizer interface allows formation of an EDLC at the two plasticizer interfaces and a rapid reinsertion into the cathode on discharge constrained only by the Li conductivity in the cathode host. The charge/discharge processes are unconventional; the ionic component of the chemical reaction between the two electrodes is driven by electrode–electrolyte interactions while the electronic component remains directly between the two electrodes via the external circuit, as is made evident by lighting of LEDs in the load. The charge/discharge is fast and efficient because the ions of the chemical reaction are only displaced a comparatively small distance across or at an interface.

ASSOCIATED CONTENT

S Supporting Information

The Supporting Information is available free of charge on the ACS Publications website at DOI: [10.1021/jacs.8b02322](https://doi.org/10.1021/jacs.8b02322).

Neutron powder diffraction data and Rietveld refinement for the layered-spinel active cathode material and SEM/EDS photomicrographs/maps of the cathode with and without SN and the Li^+ -glass electrolyte and paper matrix (cellulose); electrochemical/electrostatic charge/discharge data for five additional cells; a wide overview on the nature of self-charge including the alignments of the electrochemical potentials at the interfaces (heterojunctions) ([PDF](#))

AUTHOR INFORMATION

Corresponding Authors

*mbraga@fe.up.pt

*jgoodenough@mail.utexas.edu

ORCID

Maria Helena Braga: [0000-0003-4577-2154](https://orcid.org/0000-0003-4577-2154)

Chandrasekar M Subramaniyam: [0000-0002-8909-8846](https://orcid.org/0000-0002-8909-8846)

John B. Goodenough: [0000-0001-9350-3034](https://orcid.org/0000-0001-9350-3034)

Notes

The authors declare no competing financial interest.

ACKNOWLEDGMENTS

This work is the product of a collaborative research project between the University of Porto, Portugal, and The University of Texas at Austin. The authors would like to acknowledge Professor G. Yu for allowing us to use his laboratory. M.H.B. acknowledges the COMPETE2020 and FCT project, EU and Portugal, PTDC/CTM-ENE/2391/2014.

REFERENCES

- (1) Choi, N.-S.; Han, J.-G.; Ha, S.-Y.; Parka, I.; Back, C.-K. *RSC Adv.* **2015**, *5*, 2732–2748.
- (2) Braga, M. H.; Stockhausen, V.; Ferreira, J. A.; Oliveira, J. C. E.; El-Azab, A. *J. Mater. Chem. A* **2014**, *2*, 5470–5480.

- (3) Braga, M. H.; Murchison, A. J.; Ferreira, J. A.; Singh, P.; Goodenough, J. B. *Energy Environ. Sci.* **2016**, *9* (3), 948–954.
- (4) Braga, M. H.; Grundish, N. S.; Murchison, A. J.; Goodenough, J. B. *Energy Environ. Sci.* **2017**, *10*, 331–336.
- (5) Braga, M. H.; Murchison, A. J.; Oliveira, J. E.; Ferreira, J. A.; Goodenough, J. B. Self-Charging and Self-Cycling of All-Solid-State Electrochemical Cells. Submitted for publication.
- (6) Alarco, P. J.; Abu-Lebdeh, Y.; Abouimran, A.; Armand, M. *Nat. Mater.* **2004**, *3*, 476–481.
- (7) Liss, K.-D.; Hunter, B.; Hagen, M.; Noakes, T.; Kennedy, S. *Phys. B* **2006**, *385–386* (2), 1010–1012.
- (8) Das, S.; Prathapa, S. J.; Menezes, P. V.; Guru Row, T. N.; Bhattacharyya, A. J. *J. Phys. Chem. B* **2009**, *113* (15), 5025–5031.
- (9) Moorhead-Rosenberg, Z.; Shin, D. W.; Chemelewski, K. R.; Goodenough, J. B.; Manthiram, A. *Appl. Phys. Lett.* **2012**, *100*, 213909.
- (10) Song, J.; Shin, D. W.; Lu, Y.; Amos, C. D.; Manthiram, A.; Goodenough, J. B. *Chem. Mater.* **2012**, *24* (15), 3101–3109.
- (11) Liu, G.; Park, K.-S.; Song, J.; Goodenough, J. B. *J. Power Sources* **2013**, *243*, 260–266.
- (12) Lee, E.-S.; Huq, A.; Chang, H.-Y.; Manthiram, A. *Chem. Mater.* **2012**, *24* (3), 600–612.
- (13) Mancini, M.; Axmann, P.; Gabrielli, G.; Kinyanjui, M.; Kaiser, U.; Wohlfahrt-Mehrens, M. *ChemSusChem* **2016**, *9*, 1843–1849.
- (14) Braga, M. H.; Ferreira, J. A.; Murchison, A. J.; Goodenough, J. B. *J. Electrochem. Soc.* **2017**, *164* (2), A207–A213.